This Accepted Manuscript has not been copyedited and formatted. The final version may differ from this version. A link to any extended data will be provided when the final version is posted online.

eNeuro

Research Article: Methods/New Tools | Novel Tools and Methods

Embryonic neocortical microglia express Toll-like receptor 9 and respond to plasmid DNA injected into the ventricle: technical considerations regarding microglial distribution in electroporated brain walls

Yuki Hattori[1,2] and Takaki Miyata[1]

[1]*Department of Anatomy and Cell Biology, Nagoya University Graduate School of Medicine, Nagoya, Japan*
[2]*Research Fellow of Japan Society for the Promotion of Science*

https://doi.org/10.1523/ENEURO.0312-18.2018

Received: 9 August 2018

Revised: 19 October 2018

Accepted: 27 October 2018

Published: 16 November 2018

Author Contributions: YH and TM designed research and wrote the paper; YH performed the experiments and analyzed the data. Both authors approved the final version of the manuscript.

Funding: http://doi.org/10.13039/501100001691Japan Society for the Promotion of Science (JSPS)
16J06207
18K15003
16H02457
16K15169

The authors declare no competing financial interests.

JSPS KAKENHI Grant numbers 16H02457 and 16K15169 [T. Miyata]. JSPS KAKENHI Grant numbers 16J06207 (Grant-in-Aid for JSPS Fellows) [Y. Hattori] and 18K15003 (Grant-in-Aid for Young Scientists) [Y. Hattori].

Corresponding Author: Yuki Hattori, Department of Anatomy and Cell Biology, Nagoya University Graduate School of Medicine, 65 Tsurumai, Showa, Aichi, Nagoya, Japan. E-mail: ha-yuki@med.nagoya-u.ac.jp.

Cite as: eNeuro 2018; 10.1523/ENEURO.0312-18.2018

Alerts: Sign up at www.eneuro.org/alerts to receive customized email alerts when the fully formatted version of this article is published.

Accepted manuscripts are peer-reviewed but have not been through the copyediting, formatting, or proofreading process.

Copyright © 2018 Hattori and Miyata
This is an open-access article distributed under the terms of the Creative Commons Attribution 4.0 International license, which permits unrestricted use, distribution and reproduction in any medium provided that the original work is properly attributed.

eNeuro Accepted Manuscript

eNeuro Accepted Manuscript

1. **Manuscript Title:** Embryonic neocortical microglia express Toll-like receptor 9 and respond to plasmid DNA injected into the ventricle: technical considerations regarding microglial distribution in electroporated brain walls
2. **Abbreviated Title:** Microglia expressing TLR9 respond to plasmid DNA

3. **List all Autor Names and Affiliations:** Yuki Hattori[1,2,*], Takaki Miyata[1]
[1] Department of Anatomy and Cell Biology, Nagoya University Graduate School of Medicine, Nagoya, Japan
[2] Research Fellow of Japan Society for the Promotion of Science

4. **Author Contributions:** YH and TM designed research and wrote the paper; YH performed the experiments and analyzed the data. Both authors approved the final version of the manuscript.

5. **Corresponding Author:** Yuki Hattori
Department of Anatomy and Cell Biology, Nagoya University Graduate School of Medicine, Nagoya, Japan.
65 Tsurumai, Showa, Aichi, Nagoya, Japan
E-mail: ha-yuki@med.nagoya-u.ac.jp

6. **Number of figures:** 8
7. **Number of tables:** 7
8. **Number of multimedia:** 2
9. **Number of extended data figures:** 2
10. **Number of words for Abstract:** 249
11. **Number of words for Significance Statement:** 117
12. **Number of words for Introduction:** 362
13. **Number of words for Discussion:** 671

14. **Acknowledgements:** We thank Makoto Masaoka and Namiko Noguchi (Department of Anatomy and Cell Biology, Nagoya University Graduate School of Medicine) for technical assistance. This work was supported by Japan Society for the Promotion of Science (JSPS) KAKENHI Grant numbers 16H02457 and 16K15169 [T. Miyata] and JSPS KAKENHI Grant numbers 16J06207 (Grant-in-Aid for JSPS Fellows) [Y. Hattori] and 18K15003 (Grant-in-Aid for Young Scientists) [Y. Hattori].

15. **Conflict of Interest:**

A. No (The authors declare no competing financial interests.)

16. **Funding sources**
JSPS KAKENHI Grant numbers 16H02457 and 16K15169 [T. Miyata]
JSPS KAKENHI Grant numbers 16J06207 (Grant-in-Aid for JSPS Fellows) [Y. Hattori] and 18K15003 (Grant-in-Aid for Young Scientists) [Y. Hattori]

eNeuro Accepted Manuscript

Abstract

Microglia, the resident immune cells in the central nervous system, play multiple roles during development. In the embryonic cerebral wall, microglia modulate the functions of neural stem/progenitor cells through their distribution in regions undergoing cell proliferation and/or differentiation. Previous studies using CX3CR1-GFP transgenic mice demonstrated that microglia extensively survey these regions. To simultaneously visualize microglia and neural-lineage cells that interact with each other, we applied the *in utero* electroporation (IUE) technique, which has been widely used for gene-transfer in neurodevelopmental studies, to CX3CR1-GFP mice (males and females). However, we unexpectedly faced a technical problem: although microglia are normally distributed homogeneously throughout the mid-embryonic cortical wall with only limited luminal entry, the intraventricular presence of exogenously derived plasmid DNAs induced microglia to accumulate along the apical surface of the cortex and aggregate in the choroid plexus. This effect was independent of capillary needle puncture of the brain wall or application of electrical pulses. The microglial response occurred at plasmid DNA concentrations lower than those routinely used for IUE, and was mediated by activation of Toll-like receptor 9 (TLR9), an innate immune sensor that recognizes unmethylated cytosine-phosphate guanosine (CpG) motifs abundant in microbial DNA. Administration of plasmid DNA together with oligonucleotide (ODN) 2088, the antagonist of TLR9, restored the normal (dispersed) intramural localization of microglia and decreased luminal accumulation of these cells. Thus, via TLR9, intraventricular plasmid DNA administration causes aberrant distribution of embryonic microglia, suggesting that the behavior of microglia in brain primordia subjected to IUE should be carefully interpreted.

(249 words)

eNeuro Accepted Manuscript

Significance statement

Microglia have been recently shown to play multiple roles in the embryonic brain. In the trials for labeling neural-lineage cells using IUE technique in CX3CR1-GFP mice, in which microglia express GFP, to achieve dual live-imaging of these cell types, we unexpectedly found that intra-ventricular administration of plasmid DNA caused microglial aberrant accumulation along the luminal surface of the cerebral wall and in the choroid plexus. Notably, Co-administration of TLR9 antagonist into the ventricle together with plasmid DNA restored the normal dispersed localization of microglia in the mid-embryonic (E14) cortex, suggesting that massive microglial accumulation induced by plasmid DNA is primarily mediated by TLR9 activation. Our findings have implications for the application of IUE to investigate embryonic microglia.

(117 words)

eNeuro Accepted Manuscript

Introduction

Microglia, the resident macrophages of the central nervous system, are distributed throughout both adult and embryonic brain (Ashwell et al., 1991; Perry et al., 1985; Nimmerjahn et al., 2005; Monier et al., 2007; Swinnen et al., 2013). Embryonic microglia play multiple roles in development of neural-lineage cells, e.g., phagocytotically eliminating $Tbr2^{+}$ intermediate progenitors (Cunningham et al., 2013; Barger et al., 2018), regulating the differentiation status of neural progenitor cells in the subventricular zone (SVZ) and ventricular zone (VZ) (Arnò et al., 2014; Hattori and Miyata, 2018), and modulating cortical interneuron positioning (Squarzoni et al., 2014; Thion and Garel, 2017). Live-imaging studies of microglia using transgenic mice such as CX3CR1-GFP mice (Jung et al., 2000) have shown that microglia dynamically change their distribution during cortical development (Swinnen et al., 2013) and extensively survey proliferative zones in response to CXCL12 during the mid-embryonic period (Hattori and Miyata, 2018).

To further investigate how microglia and neural-lineage cells interact and/or collaborate (i.e., where, when, and for how long microglia contact undifferentiated and/or intermediate neural progenitors and whether these cell types mutually influence their development), it is necessary to simultaneously live-monitor microglia and neural lineage cells and observe them under genetic manipulation. For labeling and genetic modification of neural lineage cells of embryonic mammalian brains, the *in utero* electroporation (IUE) technique has been widely used (Saito and Nakatsuji, 2001; Fukuchi-Shimogori and Grove, 2001; Tabata and Nakajima, 2001). Because this technique is easily combined with the use of transgenic mice developed for visualization of certain cell types or subcellular structures (Okamoto et al., 2013; Shinoda et al., 2018), we predicted that it would be useful for monitoring microglia in CX3CR1-GFP mice. In pilot trials of this dual imaging approach (i.e., visualization of both microglia and non-microglia), however, we unexpectedly found that conventional IUE of the embryonic mouse cerebral wall markedly altered microglial distribution in the cortex. A recent study reported that IUE caused activation of embryonic microglia, and thus induced cell death, in the developing hypothalamus (Rosin et al., 2018), but the underlying biological mechanisms remained unknown. In this study, we investigated the causes of abnormal microglial distribution and point to a potential molecular mechanism for this phenomenon.

(362 words)

eNeuro Accepted Manuscript

Materials and Methods

Mice

CX3CR1-GFP mice (Jung et al., 2000; IMSR Cat# JAX:005582, RRID:IMSR_JAX:005582) were purchased from Jackson Laboratories (Bar Harbor, ME, USA). ICR mice were purchased from Japan SLC (Shizuoka, Japan). Mice were housed under specific pathogen-free conditions at Nagoya University. All protocols for animal experiments were approved by the Institutional Animal Care and Use Committee of Nagoya University. To obtain CX3CR1-GFP^{+} embryos (heterozygous), male homozygous CX3CR1-GFP mice were mated with female ICR wild-type mice.

Plasmid DNA and LPS injection into the lateral ventricle

Plasmid DNA (pEFX2-Lyn-mCherry) purified using the QIAGEN Plasmid Maxi kit (catalog number, 12163; QIAGEN, Hilden, Germany) or the EndoFree Plasmid Maxi kit (catalog number, 12362; QIAGEN) was dissolved in Tris-EDTA (10 mM Tris-HCl, 1 mM EDTA, pH 8.0) at a concentration of 5 µg/µl. The plasmid stock was diluted in saline solution to a concentration of 0.5 µg/µl. To monitor injection, Fast Green (0.1%) was added to the plasmid DNA solution at a ratio of 1:10. One microliter of plasmid DNA solution was injected into the lateral ventricle of the right hemisphere of E12 mouse brain. The final concentration of plasmid DNA ranged 0.03–0.5 µg/µl, as indicated. After two days, the number and distribution pattern of microglia were quantified in the lateral part of the cerebral wall and choroid plexus (right hemisphere) (Fig. 1B). LPS (Sigma-Aldrich, St. Louis, MO, USA) was diluted in saline solution to obtain a concentration of 2.5 ng, 250 pg, 25 pg or 2.5 pg/µl and administered one microliter of the solution into the lateral ventricle of E12 mouse brain. Regarding the amount of bacterial endotoxin contained in plasmid DNA solution, we referred to the manufacturer's website (https://www.qiagen.com/us/resources/technologies/plasmid-resource-center/removal%20of%20bacterial%20endotoxins/)

In utero electroporation (IUE)

IUE was performed as described previously (Okamoto et al, 2013; Shinoda et al., 2018). After pregnant ICR mice were anesthetized by intraperitoneal injection of pentobarbital sodium (Somnopentyl; Kyoritsu Seiyaku, Tokyo, Japan), 1 µl of plasmid DNA solution was injected into the

eNeuro Accepted Manuscript

lateral ventricle of E12 mouse embryos. Briefly, the head of the embryo inside the uterus was placed between the disks of a forceps-type electrode (3 mm disk electrodes for E12; CUY650P3, NEPA GENE, Chiba, Japan), and electric pulses (32 V) were applied four times, resulting in gene transfection into the cerebral wall.

Administration of TLR9 antagonist together with plasmid DNA

Previous studies tested various oligonucleotides (ODNs) for their stimulatory or inhibitory activities for TLR9 (Krieg et al., 1995; Stunz et al., 2002). Based on the finding that ODN 2088 is one of the most effective inhibitors, we applied it in our experiments as TLR9 antagonist. The ODN 2088 (5'-TCC TGG CGG GGA AGT-3') was purchased from Invivogen (San Diego, CA, USA). The drug was suspended in endotoxin-free water and dissolved in plasmid DNA solution at a mass ratio of plasmid DNA/ODN 2088 1:1. Plasmid DNA and ODN 2088 were injected into the lateral ventricles of E12 embryos. After 2 days (E14), the brains were perfused with 4% PFA and subjected to immunohistochemistry.

Immunohistochemistry

Immunohistochemistry was performed as described previously (Okamoto et al., 2013). Brains were fixed in 4% PFA, immersed in 20% sucrose, and frozen-sections (16 μm thickness) were cut. Sections were treated with the following primary antibodies: rat anti-GFP (1:500, Nacalai Tesque, Kyoto, Japan; Cat# 04404-84, RRID:AB_10013361) and rabbit anti-RFP (1:500, MBL, Aichi, Japan; Cat# PM005, RRID:AB_591279). After washes, sections were treated with secondary antibodies conjugated to Alexa Fluor 488 (1:400, Molecular Probes, Eugene, OR, USA; Cat# A-11006, RRID:AB_141373) or Alexa Fluor 546 (1:400, Molecular Probes; Cat# A-11010, RRID:AB_143156) and imaged on a BX60 fluorescence microscope (Olympus, Tokyo, Japan) or FV1000 confocal microscope (Olympus). The cerebral wall was divided into 6 bins (40-μm) and numbered in an inside-out fashion (bin 1–6). We counted the number of microglia of which somas were within the VZ (including ones along the apical surface) but excluded microglia whose somata were completely in the ventricular lumen even though they partly attached to the apical surface.

Cell sorting

Freshly isolated pallial walls derived from E14 male and female CX3CR1-GFP mice were

eNeuro Accepted Manuscript

171 treated with trypsin (0.05%, 3 min at 37°C). Dissociated pallial cells were filtered through a 40-μm
172 strainer (Corning, Corning, NY, USA) to eliminate all remaining cell clumps, and then resuspended in
173 DMEM containing 5% fetal bovine serum (FBS) (Invitrogen, Waltham, MA, USA), 5% horse serum
174 (HS) (Invitrogen), and penicillin/streptomycin (50 U/ml, each) (Meiji Seika Pharma, Tokyo, Japan).
175 CX3CR1-GFP^{+} cells were sorted through a 100-μm nozzle by FACS Aria II (BD Biosciences,
176 Franklin Lakes, NJ, USA). The drop delay was optimized using BD Biosciences Accudrop™ beads
177 (BD Biosciences).
178
179 **Real-time PCR**
180 First-strand cDNA was synthesized from approximately 100 ng total RNA was
181 reverse-transcribed into cDNA using SuperScript III reverse transcriptase (Thermo Fisher Scientific,
182 Waltham, MA, USA) in the presence of RNase inhibitor (Thermo Fisher Scientific). Real-time PCR
183 was performed with SYBR Green Real Time PCR Master (Toyobo, Osaka, Japan) using Thermal
184 Cycler Dice Real Time System TP800 (TaKaRa, Shiga, Japan). To amplify specific transcripts,
185 samples were heated at 95°C for 15 min and subsequently underwent a melting curve analysis from
186 60°C to 95°C. The threshold cycle number (Ct) of the target was calculated and expressed relative to
187 that of *GAPDH*, and then ΔΔCt values of the target were calculated and presented as relative fold
188 induction. Primers were: 5′-AGC CTC CGA GAC AAC TAC CT-3′ (sense) and 5′-TTG GTC AGG
189 GCC TTT AGC TG-3′ (antisense) for *TLR9*; 5'-TCC CTG CAT AGA GGT AGT TCC TA-3' (sense)
190 and 5'-TTC AAG GGG TTG AAG CTC AGA-3' (antisense) for *TLR4*; and 5'-GTT GTC TCC TGC
191 GAC TTC A-3' (sense) and 5'-GGT GGT CCA GGG TTT CTT A-3' (antisense) for
192 glyceraldehyde-3-phosphate dehydrogenase (*GAPDH*).
193
194 **Live imaging in cortical slice culture**
195 To obtain cortical slices covered with intact meninges, whole forebrains isolated from E14
196 male and female CX3CR1-GFP mice that had been electroporated at E12 were embedded in 2%
197 agarose gel, and then sliced coronally (350 μm) using a vibratome. The slices were cultured in
198 collagen gel as previously described (Miyata et al., 2004). Time-lapse imaging was performed on a
199 CV1000 confocal microscope (Olympus). Chambers for on-stage culture were filled with 40% O_2.
200
201 **Statistical analysis**

eNeuro Accepted Manuscript

202 Quantitative data are presented as means ± S.D. from representative experiments. Statistical
203 differences between groups were analyzed by Mann–Whitney U test for two-group comparisons or
204 Steel–Dwass test for multiple comparisons using R software. $P < 0.05$ was considered significant.
205 P-values in every figure are separately listed in tables (Table 1–7). Individual values were plotted as
206 open circles in bar graphs. The number of samples examined in each analysis is shown in the figure
207 legends.
208

eNeuro Accepted Manuscript

Results

1. IUE disturbs microglial distribution in the developing cerebral cortex

To simultaneously visualize microglia and neural-lineage cells, we performed IUE on embryonic day (E)12 CX3CR1-GFP mice (Jung et al., 2000). Briefly, plasmid DNA (pEFX2-Lyn-mCherry) was injected into the lateral ventricle of the right hemisphere of E12 mouse brain using a glass capillary needle, followed by electrical pulses across the embryo's head (Fig. 1A). Surprisingly, immunohistochemical inspections 2 days later revealed that the distribution patterns of $CX3CR1^{+}$ microglia in the pallium and choroid plexus were abnormal (Fig. 1B, C). Normally at E14, microglia are distributed diffusely throughout the pallium along the radial (ventricle-to-pia) axis, and are found in the ventricular zone (VZ), subventricular zone (SVZ), and intermediate zone (IZ) (Perry et al., 1985; Ashwell et al., 1991; Monier et al., 2007; Cunningham et al., 2013; Swinnen et al., 2013). In brains subjected to IUE (hereafter, IUE brains), however, microglia were extremely scarce in both the SVZ and IZ (bins 2–4) and aberrantly accumulated along the apical surface (within 40 μm from the apical surface: bin 1) (Fig. 1C–E; Table 1), with the total number of microglia in the pallium and meningeal microglia comparable between control (non-IUE) and IUE brains (Fig. 1F, G). IUE brains also exhibited densely accumulated microglia in the choroid plexus and the ventricle, whereas no such massive luminal infiltrations were observed in non-IUE controls (Fig. 1C, H). IUE caused the same type of aberrant microglial distribution in wild-type (ICR, non-CX3CR1-GFP transgenic) mice (data not shown). These results indicate that, in our hands, the standard IUE technique disturbed the localization of microglia in a manner suggestive of an attraction from the IZ or SVZ toward the ventricular lumen.

2. Plasmid DNA injection into the ventricle, without electrical pulses, results in abnormal microglial distribution

To determine which of the steps involved in IUE (1, puncturing the cerebral wall with a glass capillary needle; 2, injection of plasmid vector DNA into the lateral ventricle; 3, electrical pulses) causes microglial aberrant accumulation, we compared the distribution of microglia between embryos subjected to each of these procedures separately. When the cerebral wall was only punctured with a glass capillary needle, but no solution was injected, microglia were still distributed homogenously throughout the cortex, as in control (non-treated) brains (Fig. 2A–D; Table 2). By contrast, brains that

eNeuro Accepted Manuscript

were intraventricularly injected with plasmid DNA (pEFX2-Lyn-mCherry) but not subjected to electrical pulses exhibited massive microglial accumulation near the ventricle in the VZ and their infiltration in the choroid plexus. On the other hand, electrical pulses alone did not result in aberrant microglial distribution. In another control group injected with Tris-EDTA solution (10 mM Tris-HCl, 1 mM EDTA, pH 8.0) alone, microglia showed normal distribution pattern in the cerebral wall and did not aggregate in the choroid plexus (Fig. 2A–D). These results strongly suggest that the presence of exogenously sourced plasmid DNAs in embryonic mouse ventricle caused abnormal microglial distribution.

3. Timing and sensitivity of microglial response to intraventricularly injected plasmid DNAs

Next, we sought to determine the sensitivity of intramural microglia to intraventricular plasmid DNAs. To compare the threshold amount of DNA required to provoke microglial responses with the amounts of DNA used in standard IUE protocols (0.5–1.0 μg per unilateral ventricular space) (Okamoto et al., 2013; Shinoda et al., 2018), we injected solutions containing various amounts of pEFX2-Lyn-mCherry (0.25 μg, 0.13 μg, 0.06 μg, and 0.03 μg) into the lateral ventricles of E12 embryos. After 2 days (E14), microglial accumulation near the ventricle was still observed in brains injected with 0.25 μg, 0.13 μg, or 0.06 μg plasmid DNA (Fig. 3A, B; Table 3), with no increase of the total number of pallial microglia (Fig. 3C). We also found dose-dependent accumulation of microglia in the choroid plexus (Fig. 3D). By contrast, in brains injected with 0.03 μg plasmid DNA, microglia were observed in a normal pattern (widely distributed from the VZ to IZ) with no accumulation in the choroid plexus. These results showed that amounts of plasmid DNA much smaller than those conventionally used for IUE can cause microglia to infiltrate toward and in the ventricular lumen.

To determine how quickly microglia infiltrate into the DNA-injected lumen, we analyzed E14 brains soon (4 h) after administration of plasmid DNA solution (0.5 μg plasmid DNA), and found that the distribution of microglia was already abnormal. Specifically, microglia had departed from their original locations (the IZ, SVZ and upper VZ) towards the apical surface (Fig. 4A, B; Table 4), although they had not yet accumulated in the choroid plexus (Fig. 4A, C). The total number of pallial microglia was comparable between plasmid DNA-treated and control brains (Fig. 4D). These results suggest that intramural microglia can immediately sense plasmid DNAs injected into the ventricle, leading to a change in their regional distribution.

eNeuro Accepted Manuscript

4. Intraventricular administration of TLR9 antagonist decreases microglial infiltration induced by plasmid DNA injection

Macrophages, including microglia, express Toll-like receptors (TLRs), prototype pattern-recognition receptors (PRRs) that recognize pathogen-associated molecular patterns (PAMPs) from microorganisms and thus initiate innate immune responses after viral or bacterial infection (Akira et al., 2004; Takeuchi and Akira, 2010; O'Neill et al., 2013; Vijay 2018). Among these receptors, TLR9 recognizes unmethylated CpG motifs, which are characteristic of bacterial and viral DNAs (Krieg et al., 1995; Hemmi et al., 2000; Bauer et a., 2001; Kumagai et al., 2008). TLR9 is expressed in microglia in the postnatal and adult brain (Doi et al., 2009; Butchi et al., 2011; Christensen et al., 2014; Matsuda et al., 2015; Cho and Hsieh, 2016; Scholtzova et al., 2017). Within cells, TLR9 primarily resides in the intracellular compartment (i.e., late-endosome/lysosome) and binds to CpG motifs after internalization of microbial DNA (Takeshita et al., 2001; Ahmad-Nejad et al., 2002; Barton et al., 2006; Chockalingam et al., 2009). Hence, we investigated whether plasmid DNA (usually produced in *Escherichia coli*) might evoke innate immune responses in microglia via TLR9.

To determine whether embryonic microglia express TLR9, we performed real-time quantitative PCR on CX3CR1-GFP^{+} microglia and CX3CR1-GFP^{-} cells (most of which are of the neural lineage) isolated by cell sorting from the cortical wall of E14 CX3CR1-GFP mice. CX3CR1^{+} microglia expressed 529-fold higher level of TLR9 compared with CX3CR1^{-} cells ($p = 0.0286$, Mann–Whitney U test) (Fig. 5A).

Next, to investigate whether microglial accumulation caused by plasmid DNA administration was mediated by TLR9, we co-injected ODN 2088, an inhibitory oligonucleotide that acts as a TLR9 antagonist (Stunz et al., 2002), into the mouse ventricle along with plasmid DNA (0.5 μg) (Fig. 5B). ODN 2088 treatment partially restored the number of microglia localized in the SVZ/IZ and significantly reduced their accumulation along the apical surface, although it did not entirely rescue abnormal distribution (the number of microglia in bin 1 was still higher than control [non-treated] or only ODN 2088–treated brains) (Fig. 5C, D; Table 5). In addition, microglial infiltration in the choroid plexus was significantly reduced in ODN 2088–treated brain but still greater than control groups (Fig. 5E). On the other hand, the total number of microglia in the cortex was comparable between brains injected with plasmid DNA alone and those co-injected with plasmid DNA and ODN 2088 (Fig. 5F). Together, these results suggest that microglia expressing TLR9 may sense intraventricularly injected plasmid DNA and subsequently accumulate near the apical surface in the VZ and in the choroid plexus.

eNeuro Accepted Manuscript

Furthermore, we confirmed that performing IUE with Lyn-mCherry vector in the presence of ODN 2088 enabled us to prepare fresh slice cultures in which CX3CR1-GFP^{+} microglia were almost normally distributed and neural-lineage cells were labeled red (Fig. 5G; Movie 1, 2).

5. Endotoxins, if contained in plasmid DNA solution, trigger microglial aberrant accumulation

Although ODN 2088 treatment partially improved microglial distribution in the embryonic brain, microglia still accumulated near the apical surface of the cerebral wall. We postulated that the presence of bacterial endotoxin, lipopolysaccharide (LPS), in plasmid preparations might influence embryonic microglia. Since CX3CR1^{+} microglia derived from E14 cerebral wall expressed TLR4, a receptor for LPS (Akira et al., 2004), much higher (290-fold higher level) than CX3CR1^{-} neural lineage cells ($p = 0.0286$, Mann–Whitney U test) (Fig. 6A), we wanted to test whether LPS might elicit microglial activation in a separate manner from TLR9 signaling, and also determine how much LPS would be required to cause microglial abnormal localization.

Our routine preparations of plasmid (QIAGEN Plasmid Maxi Kit) for IUE yields relatively pure DNA with low levels of endotoxin (9.3 endotoxin unit [EU]/μg plasmid DNA) (typically, 1 ng LPS corresponds to 1–10 EU, e.g., 0.47–4.7 ng LPS is estimated to be contained per 0.5 μg plasmid DNA). When LPS alone diluted in saline was injected into the lateral ventricles of E12 embryos, immunohistochemistry after 2 days (at E14) demonstrated that, in brains treated with 2.5 ng, 250 pg and 25 pg LPS, microglia were abnormally distributed (Fig. 6B–D; Table 6), which was coupled with an increase of the total number of pallial microglia in 2.5 ng LPS–treated cases (Fig. 6E). On the other hand, microglia showed normal localization in brains exposed to 2.5 pg LPS. This indicates that much lower levels of LPS than that contained in plasmid DNA solution to be used for IUE may substantially trigger microglial response.

We tested plasmid DNAs purified using a commercially-sourced endotoxin-free (< 0.1 EU/μg plasmid DNA) protocol according to manufacturer's instructions (QIAGEN EndoFree Plasmid Maxi Kit). Similar to ones purified with the QIAGEN Plasmid Maxi Kit, the endotoxin-free DNAs (0.5 μg, 0,25 μg) caused microglial aberrant distribution without an increase of the total number (Fig. 7A–D; Table 7), but endotoxin-free plasmid DNA did not evoke microglial responses at 0.13 μg, which was greater than 0.03 μg, a dose for DNAs obtained with the QIAGEN Plasmid Maxi Kit which would have contained more endotoxin (Fig.3). Of note, improvements in the localization of pallial microglia were much more clearly seen when ODN 2088 was co-administrated with endotoxin-free plasmid DNAs

eNeuro Accepted Manuscript

333 (0.5 μg) than used with endotoxin-containing ones (Fig. 7E–H; Table 7; Fig. 7-1), with a minor
334 microglial infiltration in the choroid plexus (Fig. 7I; Fig. 7-2).

335 Taken together, these results strongly suggest that although endotoxin can also disturb
336 microglial distribution, plasmid DNA itself is the major inducer of abnormal distribution of the
337 mid-embryonic (E14) cortical microglia through their activation of TLR9.

338

eNeuro Accepted Manuscript

Discussion

Here, we showed that injection of plasmid DNA into the lateral ventricle for IUE induced microglia to accumulate near the luminal surface and aggregate in the choroid plexus, even if electrical pulses were not applied. Notably, this aberrant distribution was triggered through recognition of plasmid DNA by TLR9 expressed in microglia (Fig. 8). Consistent with this, co-injection of a TLR9 antagonist into the ventricle along with plasmid DNA restored the normal, dispersed localization pattern of microglia.

Given that plasmid DNA injection changed the intramural distribution of microglia without changing the total number of microglia per cerebral wall, it is most likely that the observed disappearance of microglia from the IZ and SVZ and their accumulation along the ventricular surface were due to ventricle-directed migration. However, our results do not exclude the possibility that peripheral macrophages infiltrated the embryonic brain, as was very recently shown to occur in response to IUE (Rosin et al., 2018). Peripheral macrophage infiltration might underlie the microglial accumulation in the choroid plexus observed in this study. Nevertheless, it is unclear how deeply plasmid DNAs diffuse into the brain wall. We speculate that intra-VZ microglia primarily receive the DNAs and then release certain factors (i.e., cytokines and/or chemokines) that attract other microglia in the IZ or SVZ. Indeed, Rosin et al. (2018) showed that inflammatory cytokines and chemokines (such as tumor necrosis factor alpha (TNF-α), interleukin-1β (IL-1β), IL-6, MIP-2, RANTES, and MCP-1) were upregulated in embryonic brains following IUE. Although it remains to be determined whether embryonic microglia in the cortex induce these cytokines and chemokines in response to recognition of plasmid DNA, it is understood that TLR9-expressing cells secrete proinflammatory cytokines (such as TNF-α, IL-6, and IL-12) upon uptake of CpG motif–containing microbial DNA (Wagner, 2004; Rahmani and Rezaei, 2016). Thus, upregulation of cytokines and chemokines in IUE brains might be induced by TLR9-mediated recognition of plasmid DNA.

TNF-α contributes to the proliferation, differentiation, and survival of neural stem/progenitor cells in the brain (Bernardino et al., 2008; Peng et al., 2008; Lan et al., 2012; Kim et al., 2018). IL-6 promotes differentiation of cortical precursor cells into oligodendrocytes and astrocytes (Bonni et al., 1997; Gruol and Nelson, 1997; Rajan and McKay 1998; Nakanishi et al., 2007; Shigemoto-Mogami et al., 2014), activates adult astrocytes (Campbell et al., 1993), and functions as a neurotrophic and differentiation factor for neurons of the central and peripheral nervous

eNeuro Accepted Manuscript

systems (Satoh et al., 1988; Thier et al., 1999; Nakafuku et al., 1992; Murphy et al., 2000; Erta et al., 2012). Therefore, although IUE itself has no effect on apoptosis in neural lineage cells (Zhang et al., 2014; Rosin et al., 2018), we cannot exclude the possibility that cytokines produced by microglia expressing TLR9 could modify the physiological environment in IUE brain.

We showed that exposure to as little as 25 picograms of intraventricular LPS (a smaller amount than that contained in plasmid DNA solutions purified with the QIAGEN plasmid Maxi Kit) could attract microglia towards the apical surface. Importantly, although ODN 2088 co-administration coupled with endotoxin-free plasmid DNAs restored microglial aberrant distribution, it did not completely inhibit microglial aggregation in the choroid plexus, indicating that other molecular mechanisms might function for sensing plasmid DNAs. Previous studies revealed that double-stranded DNA complexed with cationic liposomes can induce type I interferon independently of CpG motifs in mouse embryonic fibroblasts and HEK293 cells, which do not express TLR9 (Ishii et al., 2006; Shirota et al., 2006). Recently, Takaoka et al. reported a cytoplasmic DNA sensor, DNA-dependent activator of IFN-regulatory factors (DAI), that recognizes double-stranded DNA and activates innate immune responses independently of TLR9 (Takaoka et al., 2007). Further studies are required to elucidate whether a TLR9-independent immune response to plasmid DNA occurs in microglia.

In summary, intraventricular plasmid DNA injection, a procedure essential for standard IUE techniques, can induce abnormal microglial behaviors in developing cortical walls. These abnormalities can be partly prevented by application of the TLR9 antagonist ODN2088. Overall, our findings emphasize that studies of embryonic microglia following IUE should be interpreted with caution.

(671 words)

eNeuro Accepted Manuscript

393 **References**

394

395 Ahmad-Nejad P, Häcker H, Rutz M, Bauer S, Vabulas RM, Wagner H (2002) Bacterial CpG-DNA and
396 lipopolysaccharides activate toll-like receptors at distinct cellular compartments. Eur J Immunol
397 32:1958–1968.
398 Akira S, Takeda K, Signalling TR (2004) Toll-like receptor signalling. Nature 4:88–88.
399 Arnò B, Grassivaro F, Rossi C, Bergamaschi A, Castiglioni V, Furlan R, Greter M, Favaro R, Comi G,
400 Becher B, Martino G, Muzio L (2014) Neural progenitor cells orchestrate microglia migration and
401 positioning into the developing cortex. Nat Commun 5.
402 Ashwell K (1991) The distribution of microglia and cell death in the fetal rat forebrain. Dev Brain Res
403 58:1–12.
404 Barger N, Keiter J, Kreutz A, Krishnamurthy A, Weidenthaler C, Martínez-Cerdeño V, Tarantal AF,
405 Noctor SC (2018) Microglia: An Intrinsic Component of the Proliferative Zones in the Fetal
406 Rhesus Monkey (Macaca mulatta) Cerebral Cortex. Cereb Cortex [Epub ahead of print].
407 Barton GM, Kagan JC, Medzhitov R (2006) Intracellular localization of Toll-like receptor 9 prevents
408 recognition of self DNA but facilitates access to viral DNA. Nat Immunol 7:49–56.
409 Bauer S, Kirschning CJ, Hacker H, Redecke V, Hausmann S, Akira S, Wagner H, Lipford GB (2001)
410 Human TLR9 confers responsiveness to bacterial DNA via species-specific CpG motif
411 recognition. Proc Natl Acad Sci 98:9237–9242.
412 Bernardino L, Agasse F, Silva B, Ferreira R, Grade S, Malva JO (2008) Tumor necrosis factor-alpha
413 modulates survival, proliferation, and neuronal differentiation in neonatal subventricular zone cell
414 cultures. Stem Cells 26:2361–2371.
415 Bonni A, Sun Y, Nadal-Vicens M, Bhatt A, Frank DA, Rozovsky I, Stahl N, Yancopoulos GD,
416 Greenberg ME (1997) Regulation of gliogenesis in the central nervous system by the JAK-STAT
417 signaling pathway. Science (80-) 278:477–483.
418 Butchi NB, Woods T, Du M, Morgan TW, Peterson KE (2011) TLR7 and TLR9 trigger distinct
419 neuroinflammatory responses in the CNS. Am J Pathol 179:783–794.
420 Campbell IL, Abraham CR, Masliah E, Kemper P, Inglis JD, Oldstone MB, Mucke L (1993) Neurologic
421 disease induced in transgenic mice by cerebral overexpression of interleukin 6. Proc Natl Acad Sci
422 90:10061–10065.
423 Cho KO, Hsieh J (2016) Microglial TLR9: Guardians of homeostatic hippocampal neurogenesis.

eNeuro Accepted Manuscript

Epilepsy Curr 16:39–40.

Chockalingam A, Brooks JC, Cameron JL, Blum LK, Leifer CA (2009) TLR9 traffics through the Golgi complex to localize to endolysosomes and respond to CpG DNA. Immunol Cell Biol 87:209–217.

Christensen LB, Woods TA, Carmody AB, Caughey B, Peterson KE (2014) Age-related differences in neuroinflammatory responses associated with a distinct profile of regulatory markers on neonatal microglia. J Neuroinflammation 11.

Cunningham C, L P, Martínez-Cerdeño V, Noctor SC (2013) Microglia Regulate the Number of Neural Precursor Cells in the Developing Cerebral Cortex. J Neurosci 33:4216–4233.

Doi Y, Mizuno T, Maki Y, Jin S, Mizoguchi H, Ikeyama M, Doi M, Michikawa M, Takeuchi H, Suzumura A (2009) Microglia activated with the toll-like receptor 9 ligand CpG attenuate oligomeric amyloid β neurotoxicity in in vitro and in vivo models of Alzheimer's disease. Am J Pathol 175:2121–2132.

Erta M, Quintana A, Hidalgo J (2012) Interleukin-6, a major cytokine in the central nervous system. Int J Biol Sci 8:1254–1266.

Fukuchi-Shimogori T, Grove EA (2001) Neocortex patterning by the secreted signaling molecute FGF8. Science (80-) 294:1071–1074.

Gruol DL, Nelson TE (1997) Physiological and pathological roles of interleukin-6 in the central nervous system. Mol Neurobiol 15:307–339.

Hattori Y, Miyata T (2018) Microglia extensively survey the developing cortex via the CXCL12/CXCR4 system to help neural progenitors to acquire differentiated properties. Genes Cells 23(10):915–922.

Hemmi H, Takeuchi O, Kawai T, Kaisho T, Sato S, Sanjo H, Matsumoto M, Hoshino K, Wagner H, Takeda K, Akira S (2000) A Toll-like receptor recognizes bacterial DNA. Nature 408:740–745.

Ishii KJ, Coban C, Kato H, Takahashi K, Torii Y, Takeshita F, Ludwig H, Sutter G, Suzuki K, Hemmi H, Sato S, Yamamoto M, Uematsu S, Kawai T, Takeuchi O, Akira S (2006) A toll-like receptor-independent antiviral response induced by double-stranded B-form DNA. Nat Immunol 7:40–48.

Jung S, Aliberti J, Graemmel P, Sunshine MJ, Kreutzberg GW, Sher A, Littman DR (2000) Analysis of Fractalkine Receptor CX3CR1 Function by Targeted Deletion and Green Fluorescent Protein Reporter Gene Insertion. Mol Cell Biol 20:4106–4114.

Kim M, Jung K, Kim I-S, Lee I-S, Ko Y, Shin JE, Park KI (2018) TNF-α induces human neural

eNeuro Accepted Manuscript

progenitor cell survival after oxygen–glucose deprivation by activating the NF-κB pathway. Exp Mol Med 50:14.

Kirschning CJ, Bauer S (2001) Toll-like receptors: Cellular signal transducers for exogenous molecular patterns causing immune responses. Int J Med Microbiol 291:251–260.

Krieg AM, Yi AK, Matson S, Waldschmidt TJ, Bishop GA, Teasdale R, Koretzky GA, Klinman DM (1995) CpG motifs in bacterial DNA trigger direct B-cell activation. Nature 374:546–549.

Kumagai Y, Takeuchi O, Akira S (2008) TLR9 as a key receptor for the recognition of DNA. Adv Drug Deliv Rev 60:795–804.

Lan X, Chen Q, Wang Y, Jia B, Sun L, Zheng J, Peng H (2012) TNF-alpha affects human cortical neural progenitor cell differentiation through the autocrine secretion of leukemia inhibitory factor. PLoS One 7:e50783.

Matsuda T, Murao N, Katano Y, Juliandi B, Kohyama J, Akira S, Kawai T, Nakashima K (2015) TLR9 signalling in microglia attenuates seizure-induced aberrant neurogenesis in the adult hippocampus. Nat Commun 6.

Miyata T, Kawaguchi A, Saito K, Kawano M, Muto T, Ogawa M (2004) Asymmetric production of surface-dividing and non-surface-dividing cortical progenitor cells. Development 131:3133–3145.

Monier A, Adle-Biassette H, Delezoide A-L, Evrard P, Gressens P, Verney C (2007) Entry and distribution of microglial cells in human embryonic and fetal cerebral cortex. J Neuropathol Exp Neurol 66:372–382.

Murphy PG, Borthwick LA, Altares M, Gauldie J, Kaplan D, Richardson PM (2000) Reciprocal actions of interleukin-6 and brain-derived neurotrophic factor on rat and mouse primary sensory neurons. Eur J Neurosci 12(6):1891–1899.

Nakafuku M, Satoh T, Kaziro Y (1992) Differentiation factors, including nerve growth factor, fibroblast growth factor, and interleukin-6, induce an accumulation of an active Ras.GTP complex in rat pheochromocytoma PC12 cells. J Biol Chem 267(27):19448–19454.

Nakanishi M, Niidome T, Matsuda S, Akaike A, Kihara T, Sugimoto H (2007) Microglia-derived interleukin-6 and leukaemia inhibitory factor promote astrocytic differentiation of neural stem/progenitor cells. Eur J Neurosci 25:649–658.

Nimmerjahn A, Kirchhoff F, Helmchen F (2005) Resting microglial cells are highly dynamic surveillants of brain parenchyma in vivo. Science 308:1314–1318

O'Neill LAJ, Golenbock D, Bowie AG (2013) The history of Toll-like receptors — redefining innate

eNeuro Accepted Manuscript

immunity. Nat Rev Immunol 13:453–460.

Okamoto M et al. (2013) TAG-1-assisted progenitor elongation streamlines nuclear migration to optimize subapical crowding. Nat Neurosci 16:1556–1566.

Peng H, Whitney N, Wu Y, Tian C, Dou H, Zhou Y, Zheng J (2008) HIV-1-infected and/or immune-activated macrophage-secreted TNF-alpha affects human fetal cortical neural progenitor cell proliferation and differentiation. Glia 56:903–916.

Perry VH, Hume DA, Gordon S (1985) Immunohistochemical localization of macrophages and microglia in the adult and developing mouse brain. Neuroscience 15:313–326.

Rahmani F, Rezaei N (2016) Therapeutic targeting of Toll-like receptors: a review of Toll-like receptors and their signaling pathways in psoriasis. Expert Rev Clin Immunol 12:1289–1298.

Rajan P, McKay RD (1998) Multiple routes to astrocytic differentiation in the CNS. J Neurosci 18:3620–3629.

Rosin, JM, Kurrasch, DM (2018) In utero electroporation induces cell death and alters embryonic microglia morphology and expression signatures in the developing hypothalamus. J Neuroinflammation 15:181.

Saito T, Nakatsuji N (2001) Efficient gene transfer into the embryonic mouse brain using in vivo electroporation. Dev Biol 240:237–246.

Satoh T, Nakamura S, Taga T, Matsuda T, Hirano T, Kishimoto T, Kaziro Y (1988) Induction of neuronal differentiation in PC12 cells by B-cell stimulatory factor 2/interleukin 6. Mol Cell Biol 8(8):3546–3549.

Scholtzova H, Do E, Dhakal S, Sun Y, Liu S, Mehta PD, Wisniewski T (2017) Innate Immunity Stimulation via Toll-Like Receptor 9 Ameliorates Vascular Amyloid Pathology in Tg-SwDI Mice with Associated Cognitive Benefits. J Neurosci 37:936–959.

Shigemoto-Mogami Y, Hoshikawa K, Goldman JE, Sekino Y, Sato K (2014) Microglia Enhance Neurogenesis and Oligodendrogenesis in the Early Postnatal Subventricular Zone. J Neurosci 34:2231–2243.

Shinoda T, Nagasaka A, Inoue Y, Higuchi R, Minami Y, Kato K, Suzuki M, Kondo T, Kawaue T, Saito K, Ueno N, Fukazawa Y, Nagayama M, Miura T, Adachi T, Miyata T (2018) Elasticity-based boosting of neuroepithelial nucleokinesis via indirect energy transfer from mother to daughter. PLoS Biol 16.

Shirota H, Ishii KJ, Takakuwa H, Klinman DM (2006) Contribution of interferon-beta to the immune

eNeuro Accepted Manuscript

activation induced by double-stranded DNA. Immunology 118:302–310.

Squarzoni P, Oller G, Hoeffel G, Pont-Lezica L, Rostaing P, Low D, Bessis A, Ginhoux F, Garel S (2014) Microglia Modulate Wiring of the Embryonic Forebrain. Cell Rep 8:1271–1279.

Stunz LL, Lenert P, Peckham D, Yi AK, Haxhinasto S, Chang M, Krieg AM, Ashman RF (2002) Inhibitory oligonucleotides specifically block effects of stimulatory CpG oligonucleotides in B cells. Eur J Immunol 32:1212–1222.

Swinnen N, Smolders S, Avila A, Notelaers K, Paesen R, Ameloot M, Brône B, Legendre P, Rigo JM (2013) Complex invasion pattern of the cerebral cortex bymicroglial cells during development of the mouse embryo. Glia 61:150–163.

Tabata H, Nakajima K (2001) Efficient in utero gene transfer system to the developing mouse brain using electroporation: Visualization of neuronal migration in the developing cortex. Neuroscience 103:865–872.

Takaoka A, Wang Z, Choi MK, Yanai H, Negishi H, Ban T, Lu Y, Miyagishi M, Kodama T, Honda K, Ohba Y, Taniguchi T (2007) DAI (DLM-1/ZBP1) is a cytosolic DNA sensor and an activator of innate immune response. Nature 448:501–505.

Takeshita F, Leifer CA, Gursel I, Ishii KJ, Takeshita S, Gursel M, Klinman DM (2001) Cutting Edge: Role of Toll-Like Receptor 9 in CpG DNA-Induced Activation of Human Cells. J Immunol 167:3555–3558.

Takeuchi O, Akira S (2010) Pattern recognition receptors and inflammation. Cell 140:805–820.

Thier M, März P, Otten U, Weis J, Rose-John S (1999) Interleukin-6 (IL-6) and its soluble receptor support survival of sensory neurons. J Neurosci Res 55(4):411–422.

Thion MS, Garel S (2017) On place and time: microglia in embryonic and perinatal brain development. Curr Opin Neurobiol 47:121–130.

Vijay K (2018) Toll-like receptors in immunity and inflammatory diseases: Past, present, and future. Int Immunopharmacol 59:391–412.

Wagner H (2004) The immunobiology of the TLR9 subfamily. Trends Immunol 25:381–386.

Zhang P, Yan Z, Wu C, Niu L, Liu N, Xu R (2014) Three puncture sites used for in utero electroporation show no significantly different negative impacts during gene transfer into the embryonic mouse brain. Neurosci Lett 578:176–181.

eNeuro Accepted Manuscript

546 **Figure legends**

547

548 **Figure 1 IUE disturbs microglial distribution in the developing cerebral cortex**

549 (A) Experimental design of IUE. Plasmid DNA (pEFX2-Lyn-mCherry) was injected into the right
550 lateral ventricle of an E12 CX3CR1-GFP mouse, and then electrical pulses were applied. After 2 days
551 (E14), the brain was fixed and subjected to immunohistochemical analysis. (B) Illustration showing
552 the approximate region of pallium, choroid plexus, and ventricular lumen for immunohistochemical
553 analyses. (C) Representative immunostaining to detect GFP (CX3CR1) and RFP (Lyn-mCherry) in
554 pallium, choroid plexus, and ventricular lumen of control and IUE brains. Broken lines show the
555 apical surface of the pallium in the upper and lower panel, and the choroid plexus in the middle panel.
556 Yellow arrowheads indicate microglia accumulated near the apical surface of the pallium, on the
557 choroid plexus and in the ventricular lumen. Scale bar, 100 μm. (D) Bin definition for
558 immunohistochemical analyses is shown. Each section in the cerebral wall was numbered from the
559 ventricle side (bin 1–6, 40-μm each). (E–G) Graphs depicting numbers of microglia in each bin
560 (40-μm × 300-μm square) (E), the total number within 240 μm from the apical surface of the pallium
561 (F), and the number of meningeal microglia (G). (H) Density of microglia adhered to the choroid
562 plexus in control vs. IUE brains. For statistical analyses, n = 10 samples obtained from 5 embryos
563 (two sections, each) were quantified. One or two littermates per dam were subjected to a series of tests.
564 Data represent means ± S.D. (***$p < 0.001$, **$p < 0.01$, *$p < 0.05$, or n.s. [not significant]; Mann–
565 Whitney U test).

566

567 **Figure 2 Plasmid DNA injection into the ventricle, without electrical pulses, results in**
568 **abnormal microglial distribution**

569 (A) Representative immunostaining for CX3CR1-GFP in the pallium and choroid plexus of mouse
570 brains subjected to puncture with a glass capillary needle, injection of plasmid DNA (shown as
571 pDNA) into the lateral ventricle, electrical pulses, or injection of Tris-EDTA solution (10 mM
572 Tris-HCl, 1 mM EDTA, pH 8.0) alone without plasmid DNA. Yellow arrowheads indicate microglia
573 accumulated near the apical surface of the cerebral wall or adhered to the choroid plexus. Broken lines
574 show the apical surface of the pallium in the upper panel and the choroid plexus in the lower panel.
575 Scale bar, 100 μm. (B, C) Graphs depicting the number of microglia positioned in each 40-μm bin (B)
576 and the total number of these cells within 240 μm from the apical surface (C) in brains that were

eNeuro Accepted Manuscript

subjected to each procedure. (D) Density of microglia adhered to the choroid plexus. For statistical analyses, n = 10 samples obtained from 5 embryos (two sections, each) were quantified. One or two littermates per dam were subjected to a series of tests. Data represent means ± S.D. (***p < 0.001, **p < 0.01, *p < 0.05, or n.s. [not significant]; Steel–Dwass test).

Figure 3 Sensitivity of microglial response to intraventricularly injected plasmid DNAs

(A) CX3CR1-GFP immunostaining showing microglial accumulation in brains injected with the indicated amount of plasmid DNA (0.25 μg, 0.13 μg, 0.06 μg, and 0.03 μg). Yellow arrowheads indicate microglia accumulated near the apical surface of the pallium and on the choroid plexus. Scale bar, 100 μm. (B, C) Graphs depicting the number of microglia positioned in each 40-μm bin (B) and the total number of these cells within 240 μm from the apical surface (C) in brains that were injected with plasmid DNA. (D) Density of microglia adhered to the choroid plexus. For statistical analyses, n = 10 samples obtained from 5 embryos (two sections, each) were quantified. One or two littermates per dam were subjected to a series of tests. Data represent means ± S.D. (***p < 0.001, **p < 0.01, *p < 0.05, or n.s. [not significant]; Steel–Dwass test).

Figure 4 Microglia immediately sense plasmid DNAs injected into the ventricle

(A) Representative immunostaining of CX3CR1-GFP in E14 brain fixed soon (4 hr) after administration of 0.5 μg plasmid DNA. Yellow arrowheads show microglia accumulated near the apical surface of the pallium and on the choroid plexus. Scale bar, 100 μm. (B) Graph showing the number of pallial microglia positioned in each 40-μm bin in control and plasmid-injected brains. (C) Graph comparing density of microglia adhered to choroid plexus. (D) The total number of pallial microglia within 240 μm from the apical surface. For statistical analyses, n = 10 samples obtained from 5 embryos (two sections, each) were quantified. Two or three littermates per dam were subjected to a series of tests. Data represent means ± S.D. (***p < 0.001, **p < 0.01, *p < 0.05, or n.s. [not significant]; Mann–Whitney U test).

Figure 5 Intraventricular administration of TLR9 antagonist decreases microglial infiltration induced by plasmid DNA injection

(A) Relative expression of *TLR9* (normalized against *GAPDH*) in FACS-isolated CX3CR1^{-} and CX3CR1^{+} cells derived from the cerebral wall of E14 CX3CR1-GFP mice. Data represent means ±

eNeuro Accepted Manuscript

S.D. (n = 4 samples obtained from independent experiments; p = 0.0286, Mann–Whitney U test). (B) Experimental design for ODN 2088 treatment. ODN 2088 was injected together with plasmid DNA into the lateral ventricle of E12 CX3CR1-GFP mice, and after 2 days (E14) the embryonic brains were fixed. (C) Immunofluorescence with anti-GFP antibody, showing the distribution of microglia in the pallium and choroid plexus. Yellow arrowheads indicate microglia aberrantly accumulated on the apical surface of the pallium or in the choroid plexus. Cyan arrowheads show microglia which were almost homogenously distributed in the cerebral wall. Scale bar, 100 μm. (D, E) Graphs indicate the number of CX3CR1-GFP^{+} cells in each 40-μm bin of the pallium (D) and density of microglia directly adhered to the choroid plexus (E), comparing control, only ODN 2088-treated, plasmid DNA-injected, and plasmid DNA + ODN 2088–co-injected brains. (F) Graph showing the total number of pallial microglia within 240 μm from the apical surface. (G) Double immunofluorescence for GFP (CX3CR1) and RFP (Lyn-mCherry) in the cortex of IUE E14 brain treated with ODN 2088. Microglia exhibited a normal distribution pattern in the Lyn-mCherry expressing region where IUE succeeded (refer to Movie 5-1, 5-2). Scale bar, 100 μm. For statistical analyses in D–F, n = 16 samples obtained from 8 embryos (two sections, each) were quantified. Two or three littermates per dam were subjected to a series of tests. Data represent means ± S.D. (***p < 0.001, **p < 0.01, *p < 0.05, or n.s. [not significant]; Steel–Dwass test).

Figure 6 Endotoxins trigger microglial aberrant accumulation

(A) Relative expression of *TLR4* (normalized against *GAPDH*) in FACS-isolated CX3CR1^{-} and CX3CR1^{+} cells derived from the cerebral wall of E14 CX3CR1-GFP mice. Data represent means ± S.D. (n = 4 samples obtained from independent experiments; p = 0.0286, Mann–Whitney U test). (B) Immunofluorescence with anti-GFP antibody, showing the distribution of microglia in the pallium and choroid plexus in brains injected with the indicated amount of LPS (2.5 ng, 250 pg, 25 pg, and 2.5 pg). Yellow arrowheads indicate microglia accumulated near the apical surface of the pallium and on the choroid plexus. Scale bar, 100 μm. (C, D) Graphs depicting the number of pallial microglia positioned in each bin (C) and density of microglia adhered to the choroid plexus (D) in brains treated with various amounts of LPS. (E) The total number of pallial microglia within 240 μm from the apical surface. For statistical analyses in C–E, n = 10 samples obtained from 5 embryos (two sections, each) were quantified. One or Two littermates per dam were subjected to a series of tests. Data represent means ± S.D. (***p < 0.001, **p < 0.01, *p < 0.05, or n.s. [not significant]; Steel–Dwass test).

eNeuro Accepted Manuscript

Figure 7 Plasmid DNA itself elicits microglial response via TLR9

(A) Immunofluorescence with anti-GFP antibody, showing the distribution of microglia in the pallium and choroid plexus in brains injected with the indicated amount of endotoxin-free plasmid DNA (0.5 μg, 0.25 μg, and 0.13 μg). Yellow arrowheads show microglia accumulated near the apical surface and on the choroid plexus. Scale bar, 100 μm. (B, C) Graphs depicting the number of pallial microglia positioned in each 40-μm bin (B) and the total number of these cells within 240 μm from the apical surface (C). (D) Density of microglia adhered to the choroid plexus. For statistical analyses in B–D, n = 10 samples obtained from 5 embryos (two sections, each) were quantified. Two or three littermates per dam were subjected to a series of tests. Data represent means ± S.D. (***$p < 0.001$, **$p < 0.01$, *$p < 0.05$, or n.s. [not significant]; Steel–Dwass test) (refer to Fig. 7-1). (E) Experimental design for administration of ODN 2088 together with endotoxin-free plasmid DNA. (F) CX3CR1-GFP immunostaining showing microglial distribution in brains injected with endotoxin-free plasmid DNA and ODN 2088–co-injected brains. Yellow arrowhead indicates microglia adhered to the choroid plexus. Cyan arrowheads show microglia which were almost homogenously distributed in the cerebral wall. Scale bar, 100 μm. (G, H) Graphs depicting the number of pallial microglia positioned in each bin (G) and the total number of these cells within 240 μm from the apical surface (H). (I) Density of microglia adhered to the choroid plexus. For statistical analyses in G–I, n = 16 samples obtained from 8 embryos (two sections, each) were quantified. Two or three littermates per dam were subjected to a series of tests. Data represent means ± S.D. (***$p < 0.001$, **$p < 0.01$, *$p < 0.05$, or n.s. [not significant]; Steel–Dwass test) (refer to Fig. 7-2).

Figure 8 Schematic summary

Schematic illustration showing the mechanism underlying the aberrant distribution of microglia in the cerebral wall of IUE-performed brain. The presence of exogenously derived plasmid DNAs induced microglia to accumulate along the apical surface of the cerebral wall and aggregate in the choroid plexus. This effect was independent of capillary needle puncture of the brain wall, or application of electrical pulses. Such microglial response is mediated by activation of TLR9, which is expressed intracellularly in microglia.

eNeuro Accepted Manuscript

Extended data (Multimedia)

Movie 1 Live-imaging of microglia in plasmid DNA–treated brains

Live imaging of microglia in a cortical slice derived from a CX3CR1-GFP mouse brain transfected with Lyn-mCherry. Time-lapse imaging covers a period of 10 hr (1 image/10 min). Green, CX3CR1-GFP. Magenta, Lyn-mCherry. Scale bar, 100 μm.

Movie 2 Live-imaging of microglia in plasmid DNA and ODN 2088–coinjected brains

Live imaging of microglia in a cortical slice derived from a CX3CR1-GFP mouse brain transfected Lyn-mCherry with co-administration of ODN 2088. Time-lapse imaging covers a period of 10 hr (1 image/10 min). Green, CX3CR1-GFP. Magenta, Lyn-mCherry. Scale bar, 100 μm.

Extended data figures

Figure 7-1

Graph depicting the number of pallial microglia positioned in each 40-μm bin comparing six groups, Fig. 5D Cont., Fig. 5D plasmid DNA, Fig. 5D plasmid DNA + ODN 2088, Fig. 7G Cont., Fig. 7G endotoxin-free plasmid DNA, and Fig. 7G endotoxin-free plasmid DNA + ODN 2088. Data represent means ± S.D. (Steel–Dwass test).

Figure 7-2

Graph showing density of microglia adhered to the choroid plexus comparing six groups, Fig. 5E Cont., Fig. 5E plasmid DNA, Fig. 5E plasmid DNA + ODN 2088, Fig. 7I Cont., Fig. 7I endotoxin-free plasmid DNA, and Fig. 7I endotoxin-free plasmid DNA + ODN 2088. Data represent means ± S.D. (Steel–Dwass test).

eNeuro Accepted Manuscript

Tables

Table 1 Statistics in Figure 1

Graph	Data structure	Type of test	p value
Fig. 1E	Non-parametric	Mann–Whitney U test	bin 1, $p = 1.1 \times 10^{-5}$; bin 2, p = 0.0022; bin 3, p = 0.0307; bin 4, p = 0.0014; bin 5, p = 0.4281; bin 6, p = 0.0495
Fig. 1F	Non-parametric	Mann–Whitney U test	p = 0.6835
Fig. 1G	Non-parametric	Mann–Whitney U test	p = 0.1021
Fig. 1H	Non-parametric	Mann–Whitney U test	$p = 1.1 \times 10^{-5}$

Table 2 Statistics in Figure 2

Graph	Data structure	Type of test	p value
Fig. 2B, bin 1	Non-parametric	Steel–Dwass test	Cont. vs. Puncture only, p = 0.9990; Cont. vs. pDNA injection, p = 0.0011; Cont. vs. Electrical shock only, p = 0.9973; Cont. vs. TE buffer injection, p = 0.9871
Fig. 2B, bin 2	Non-parametric	Steel–Dwass test	Cont. vs. Puncture only, p = 0.9781; Cont. vs. pDNA injection, p = 0.0369; Cont. vs. Electrical shock only, p = 0.9937; Cont. vs. TE buffer

eNeuro Accepted Manuscript

			injection, p = 0.9996
Fig. 2B, bin 3	Non-parametric	Steel–Dwass test	Cont. vs. Puncture only, p = 1.0000; Cont. vs. pDNA injection, p = 0.0055; Cont. vs. Electrical shock only, p = 0.9976; Cont. vs. TE buffer injection, p = 0.9976
Fig. 2B, bin 4	Non-parametric	Steel–Dwass test	Cont. vs. Puncture only, p = 0.9992; Cont. vs. pDNA injection, p = 0.0154; Cont. vs. Electrical shock only, p = 0.9964; Cont. vs. TE buffer injection, p = 0.9996
Fig. 2B, bin 5	Non-parametric	Steel–Dwass test	Cont. vs. Puncture only, p = 0.9473; Cont. vs. pDNA injection, p = 0.1056; Cont. vs. Electrical shock only, p = 0.9976; Cont. vs. TE buffer injection, p = 1.0000
Fig. 2B, bin 6	Non-parametric	Steel–Dwass test	Cont. vs. Puncture only, p = 0.9998; Cont. vs. pDNA injection, p = 0.3261; Cont. vs. Electrical shock only, p = 0.9962;

eNeuro Accepted Manuscript

			Cont. vs. TE buffer injection, p = 1.0000
Fig. 2C	Non-parametric	Steel–Dwass test	Cont. vs. Puncture only, p = 0.9994; Cont. vs. pDNA injection, p = 1.0000; Cont. vs. Electrical shock only, p = 0.9969; Cont. vs. TE buffer injection, p = 0.9981
Fig. 2D	Non-parametric	Steel–Dwass test	Cont. vs. Puncture only, p = 0.9989; Cont. vs. pDNA injection, p = 0.0015; Cont. vs. Electrical shock only, p = 0.9994; Cont. vs. TE buffer injection, p = 0.9913

701

702 **Table 3 Statistics in Figure 3**

Graph	Data structure	Type of test	p value
Fig. 3B, bin 1	Non-parametric	Steel–Dwass test	Cont. vs. 0.25 µg, p = 0.0013; Cont. vs. 0.13 µg, p = 0.0013; Cont. vs. 0.06 µg, p = 0.0028; Cont. vs. 0.03 µg, p = 0.8787
Fig. 3B, bin 2	Non-parametric	Steel–Dwass test	Cont. vs. 0.25 µg, p = 0.0693;

eNeuro Accepted Manuscript

			Cont. vs. 0.13 µg, p = 0.0453; Cont. vs. 0.06 µg, p = 0.9317; Cont. vs. 0.03 µg, p = 0.9990
Fig. 3B, bin 3	Non-parametric	Steel–Dwass test	Cont. vs. 0.25 µg, p = 0.1044; Cont. vs. 0.13 µg, p = 0.2141; Cont. vs. 0.06 µg, p = 0.8898; Cont. vs. 0.03 µg, p = 0.8352
Fig. 3B, bin 4	Non-parametric	Steel–Dwass test	Cont. vs. 0.25 µg, p = 0.0098; Cont. vs. 0.13 µg, p = 0.0196; Cont. vs. 0.06 µg, p = 0.3581; Cont. vs. 0.03 µg, p = 0.9985
Fig. 3B, bin 5	Non-parametric	Steel–Dwass test	Cont. vs. 0.25 µg, p = 0.8286; Cont. vs. 0.13 µg, p = 0.7255; Cont. vs. 0.06 µg, p = 0.8286; Cont. vs. 0.03 µg, p = 1.0000
Fig. 3B, bin 6	Non-parametric	Steel–Dwass test	Cont. vs. 0.25 µg, p =

eNeuro Accepted Manuscript

			0.4412; Cont. vs. 0.13 µg, p = 0.4412; Cont. vs. 0.06 µg, p = 0.9667; Cont. vs. 0.03 µg, p = 0.9999
Fig. 3C	Non-parametric	Steel–Dwass test	Cont. vs. 0.25 µg, p = 0.6147; Cont. vs. 0.13 µg, p = 0.9493; Cont. vs. 0.06 µg, p = 0.7574; Cont. vs. 0.03 µg, p = 0.9162
Fig. 3D	Non-parametric	Steel–Dwass test	Cont. vs. 0.25 µg, p = 0.0015; Cont. vs. 0.13 µg, p = 0.0015; Cont. vs. 0.06 µg, p = 0.0015; Cont. vs. 0.03 µg, p = 0.1825

703

704 **Table 4 Statistics for Figure 4**

Graph	Data structure	Type of test	p value

Fig. 4B	Non-parametric	Mann–Whitney U test	bin 1, $p = 1.1 \times 10^{-5}$;
			bin 2, p = 0.0074;
			bin 3, p = 0.1023;
			bin 4, p = 0.0058;
			bin 5, p = 0.0837;

eNeuro Accepted Manuscript

			bin 6, p = 0.0275
Fig. 4C	Non-parametric	Mann–Whitney U test	p = 0.9869
Fig. 4D	Non-parametric	Mann–Whitney U test	p = 0.2789

705

706 **Table 5 Statistics in Figure 5**

Graph	Data structure	Type of test	p value
Fig. 5D, bin 1	Non-parametric	Steel–Dwass test	Cont. vs. ODN 2088, p = 0.8335; Cont. vs. pDNA, p = 5.6×10^{-6}; pDNA vs. pDNA + ODN 2088, p = 2.4×10^{-4}; Cont. vs. pDNA + ODN 2088, p = 2.1×10^{-5}
Fig. 5D, bin 2	Non-parametric	Steel–Dwass test	Cont. vs. ODN 2088, p = 0.6401; Cont. vs. pDNA, p = 1.3×10^{-5}; pDNA vs. pDNA + ODN 2088, p = 0.0627; Cont. vs. pDNA + ODN 2088, p = 0.0163
Fig. 5D, bin 3	Non-parametric	Steel–Dwass test	Cont. vs. ODN 2088, p = 0.9781; Cont. vs. pDNA, p = 8.2×10^{-5}; pDNA vs. pDNA + ODN 2088, p = 4.7×10^{-4};

eNeuro Accepted Manuscript

			Cont. vs. pDNA + ODN 2088, p = 0.5691
Fig. 5D, bin 4	Non-parametric	Steel–Dwass test	Cont. vs. ODN 2088, p = 0.9746; Cont. vs. pDNA, p = 0.0102; pDNA vs. pDNA + ODN 2088, p = 0.1967; Cont. vs. pDNA + ODN 2088, p = 0.3568
Fig. 5D, bin 5	Non-parametric	Steel–Dwass test	Cont. vs. ODN 2088, p = 0.9276; Cont. vs. pDNA, p = 0.0610; pDNA vs. pDNA + ODN 2088, p = 0.7661; Cont. vs. pDNA + ODN 2088, p = 0.5053
Fig. 5D, bin 6	Non-parametric	Steel–Dwass test	Cont. vs. ODN 2088, p = 0.9955; Cont. vs. pDNA, p = 0.9158; pDNA vs. pDNA + ODN 2088, p = 0.7539; Cont. vs. pDNA + ODN 2088, p = 0.9840
Fig. 5E	Non-parametric	Steel–Dwass test	Cont. vs. ODN 2088, p = 0.8121; Cont. vs. pDNA, p = 8.4×10^{-6}; pDNA vs. pDNA +

eNeuro Accepted Manuscript

			ODN 2088, p = 0.0374; Cont. vs. pDNA + ODN 2088, p = 8.4 × 10^{-6}
Fig. 5F	Non-parametric	Steel–Dwass test	Cont. vs. ODN 2088, p = 0.9966; Cont. vs. pDNA, p = 0.9982; pDNA vs. pDNA + ODN 2088, p = 0.6688; Cont. vs. pDNA + ODN 2088, p = 0.7716

707

708 **Table 6 Statistics in Figure 6**

Graph	Data structure	Type of test	p value
Fig. 6C, bin 1	Non-parametric	Steel–Dwass test	Cont. vs. 2.5 ng, p = 0.0012; Cont. vs. 250 pg, p = 0.0021; Cont. vs. 25 pg, p = 0.0055; Cont. vs. 2.5 pg, p = 0.7868
Fig. 6C, bin 2	Non-parametric	Steel–Dwass test	Cont. vs. 2.5 ng, p = 0.4164; Cont. vs. 250 pg, p = 0.8867; Cont. vs. 25 pg, p = 1.0000; Cont. vs. 2.5 pg, p = 0.9924

eNeuro Accepted Manuscript

Fig. 6C, bin 3	Non-parametric	Steel–Dwass test	Cont. vs. 2.5 ng, p = 0.3094; Cont. vs. 250 pg, p = 0.9889; Cont. vs. 25 pg, p = 0.8691; Cont. vs. 2.5 pg, p = 0.9998
Fig. 6C, bin 4	Non-parametric	Steel–Dwass test	Cont. vs. 2.5 ng, p = 0.7372; Cont. vs. 250 pg, p = 0.9700; Cont. vs. 25 pg, p = 0.3816; Cont. vs. 2.5 pg, p = 0.9811
Fig. 6C, bin 5	Non-parametric	Steel–Dwass test	Cont. vs. 2.5 ng, p = 1.0000; Cont. vs. 250 pg, p = 0.8700; Cont. vs. 25 pg, p = 1.0000; Cont. vs. 2.5 pg, p = 0.9986
Fig. 6C, bin 6	Non-parametric	Steel–Dwass test	Cont. vs. 2.5 ng, p = 0.9278; Cont. vs. 250 pg, p = 0.6779; Cont. vs. 25 pg, p = 0.3559; Cont. vs. 2.5 pg, p =

eNeuro Accepted Manuscript

			0.9514
Fig. 6D	Non-parametric	Steel–Dwass test	Cont. vs. 2.5 ng, p = 0.0015; Cont. vs. 250 pg, p = 0.0015; Cont. vs. 25 pg, p = 0.0026; Cont. vs. 2.5 pg, p = 0.5054
Fig. 6E	Non-parametric	Steel–Dwass test	Cont. vs. 2.5 ng, p = 0.0190; Cont. vs. 250 pg, p = 0.0845; Cont. vs. 25 pg, p = 1.0000; Cont. vs. 2.5 pg, p = 0.9994

709

710 **Table 7 Statistics in Figure 7**

Graph	**Data structure**	**Type of test**	**p value**
Fig. 7B, bin 1	Non-parametric	Steel–Dwass test	Cont. vs. 0.5 µg, p = 7.4×10^{-4}; Cont. vs. 0.25 µg, p = 0.0017; Cont. vs. 0.13 µg, p = 0.9880;
Fig. 7B, bin 2	Non-parametric	Steel–Dwass test	Cont. vs. 0.5 µg, p = 0.0018; Cont. vs. 0.25 µg, p = 0.0557; Cont. vs. 0.13 µg, p =

eNeuro Accepted Manuscript

			0.9880;
Fig. 7B, bin 3	Non-parametric	Steel–Dwass test	Cont. vs. 0.5 µg, p = 0.0018; Cont. vs. 0.25 µg, p = 0.5785; Cont. vs. 0.13 µg, p = 1.0000;
Fig. 7B, bin 4	Non-parametric	Steel–Dwass test	Cont. vs. 0.5 µg, p = 0.1122; Cont. vs. 0.25 µg, p = 0.6280; Cont. vs. 0.13 µg, p = 0.9880;
Fig. 7B, bin 5	Non-parametric	Steel–Dwass test	Cont. vs. 0.5 µg, p = 0.5457; Cont. vs. 0.25 µg, p = 0.3241; Cont. vs. 0.13 µg, p = 0.8824;
Fig. 7B, bin 6	Non-parametric	Steel–Dwass test	Cont. vs. 0.5 µg, p = 0.9691; Cont. vs. 0.25 µg, p = 0.9887; Cont. vs. 0.13 µg, p = 0.9773;
Fig. 7C	Non-parametric	Steel–Dwass test	Cont. vs. 0.5 µg, p = 0.9011; Cont. vs. 0.25 µg, p = 0.9593; Cont. vs. 0.13 µg, p = 0.9994;

eNeuro Accepted Manuscript

Fig. 7D	Non-parametric	Steel–Dwass test	Cont. vs. 0.5 µg, $p = 9.0 \times 10^{-4}$; Cont. vs. 0.25 µg, $p = 9.0 \times 10^{-4}$; Cont. vs. 0.13 µg, $p = 0.7593$
Fig. 7G, bin 1	Non-parametric	Steel–Dwass test	Cont. vs. pDNA, $p = 3.0 \times 10^{-6}$; pDNA vs. pDNA + ODN 2088, $p = 5.2 \times 10^{-6}$; Cont. vs. pDNA + ODN 2088, $p = 0.0429$
Fig. 7G, bin 2	Non-parametric	Steel–Dwass test	Cont. vs. pDNA, $p = 7.0 \times 10^{-6}$; pDNA vs. pDNA + ODN 2088, $p = 1.1 \times 10^{-5}$; Cont. vs. pDNA + ODN 2088, $p = 0.4461$
Fig. 7G, bin 3	Non-parametric	Steel–Dwass test	Cont. vs. pDNA, $p = 6.9 \times 10^{-5}$; pDNA vs. pDNA + ODN 2088, $p = 4.3 \times 10^{-4}$; Cont. vs. pDNA + ODN 2088, $p = 0.2716$
Fig. 7G, bin 4	Non-parametric	Steel–Dwass test	Cont. vs. pDNA, $p = 0.0047$; pDNA vs. pDNA + ODN 2088, $p = 0.0900$;

eNeuro Accepted Manuscript

			Cont. vs. pDNA + ODN 2088, p = 0.2895
Fig. 7G, bin 5	Non-parametric	Steel–Dwass test	Cont. vs. pDNA, p = 0.5717; pDNA vs. pDNA + ODN 2088, p = 0.3952; Cont. vs. pDNA + ODN 2088, p = 0.8520
Fig. 7G, bin 6	Non-parametric	Steel–Dwass test	Cont. vs. pDNA, p = 0.9469; pDNA vs. pDNA + ODN 2088, p = 0.9472; Cont. vs. pDNA + ODN 2088, p = 0.9965
Fig. 7H	Non-parametric	Steel–Dwass test	Cont. vs. pDNA, p = 0.6872; pDNA vs. pDNA + ODN 2088, p = 0.9550; Cont. vs. pDNA + ODN 2088, p = 0.7672
Fig. 7I	Non-parametric	Steel–Dwass test	Cont. vs. pDNA, p = 2.6×10^{-5}; pDNA vs. pDNA + ODN 2088, p = 0.5896; Cont. vs. pDNA + ODN 2088, p = 9.2×10^{-5}

711

712

713

eNeuro Accepted Manuscript

Figure 1

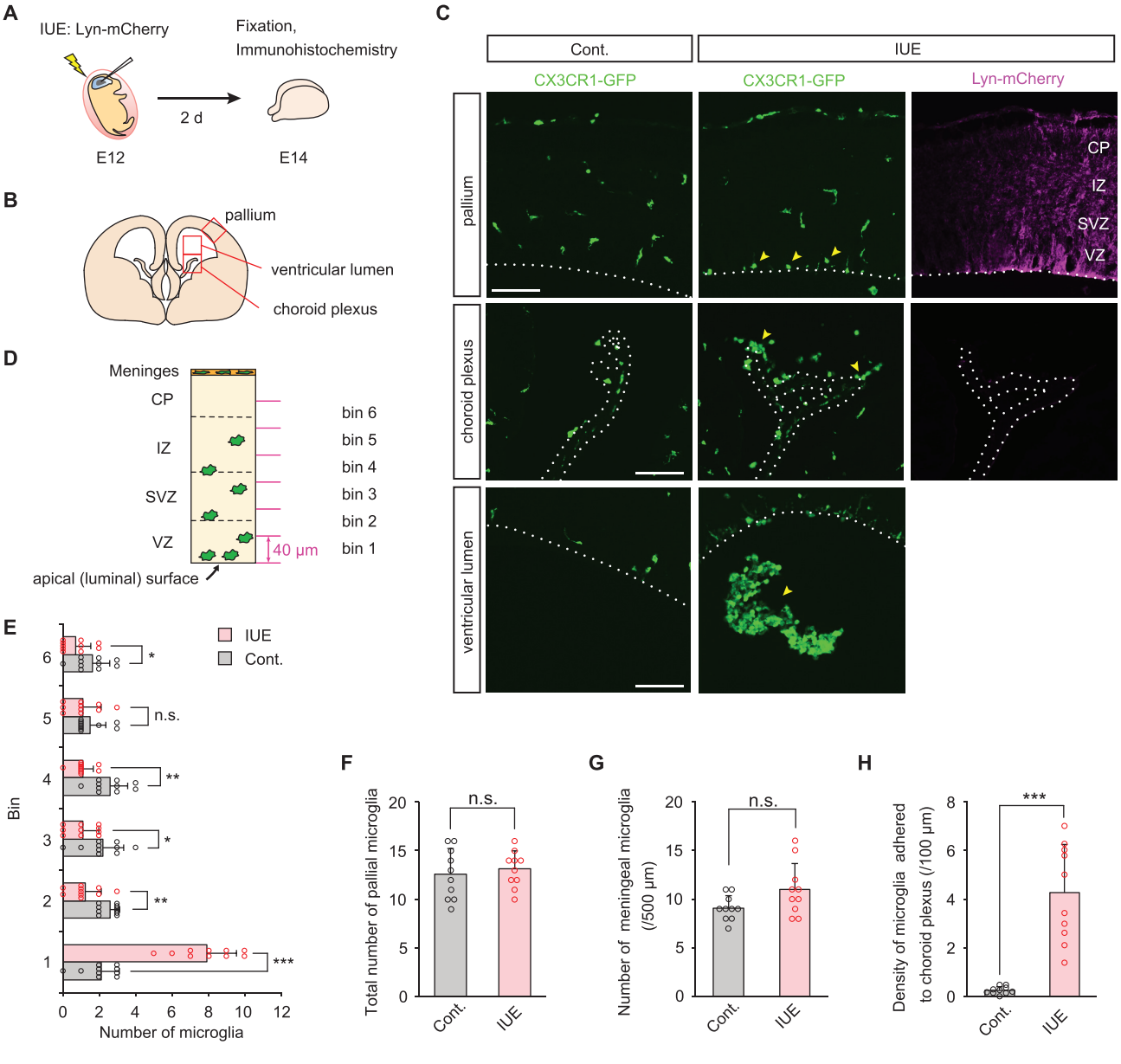

eNeuro Accepted Manuscript

Figure 2

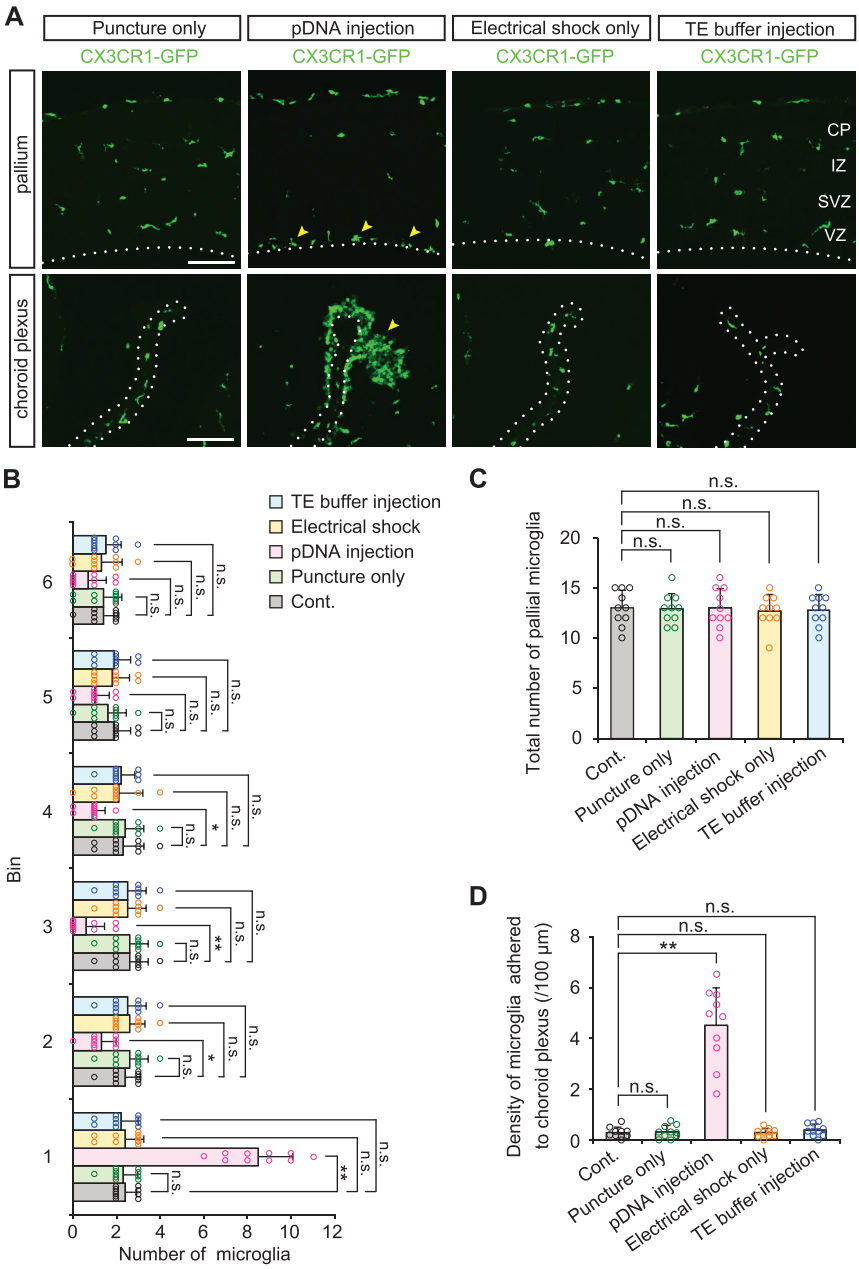

eNeuro Accepted Manuscript

Figure 3

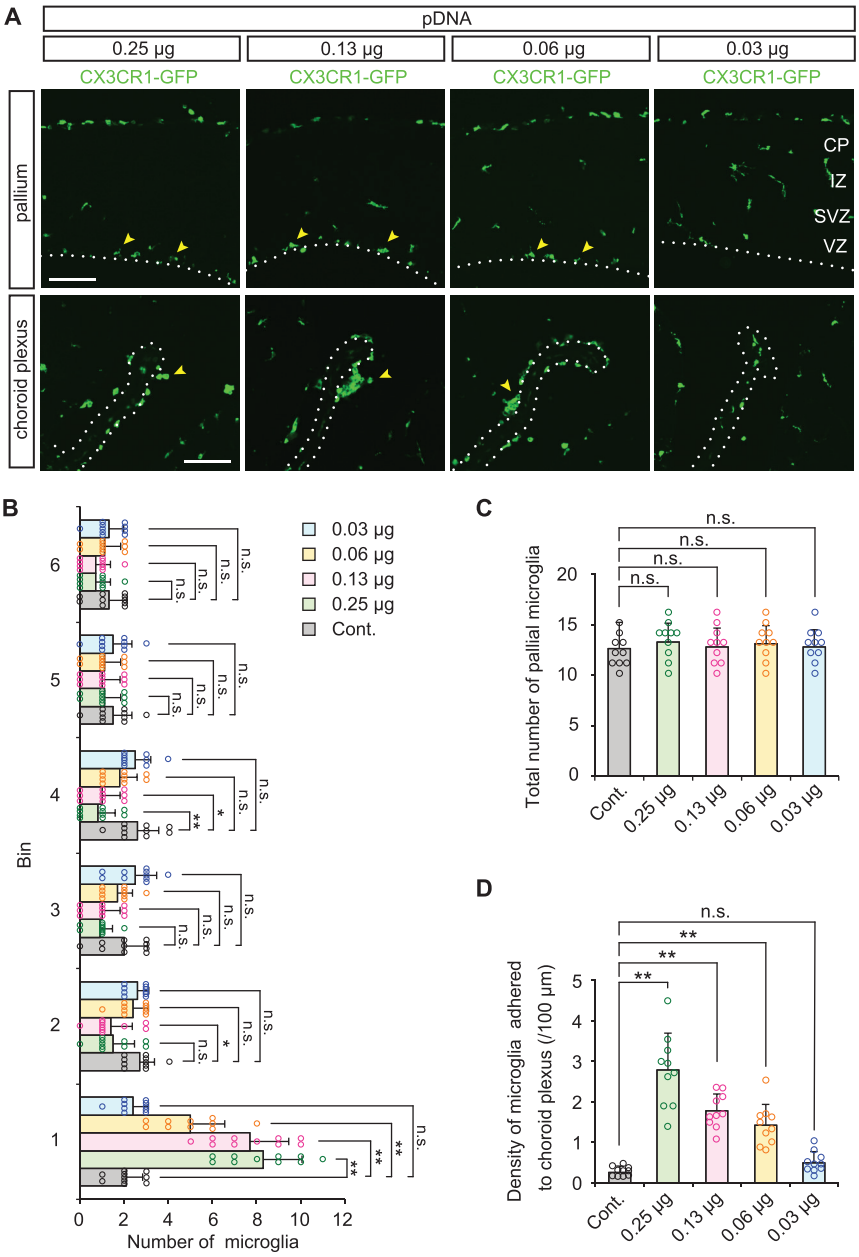

eNeuro Accepted Manuscript

Figure 4

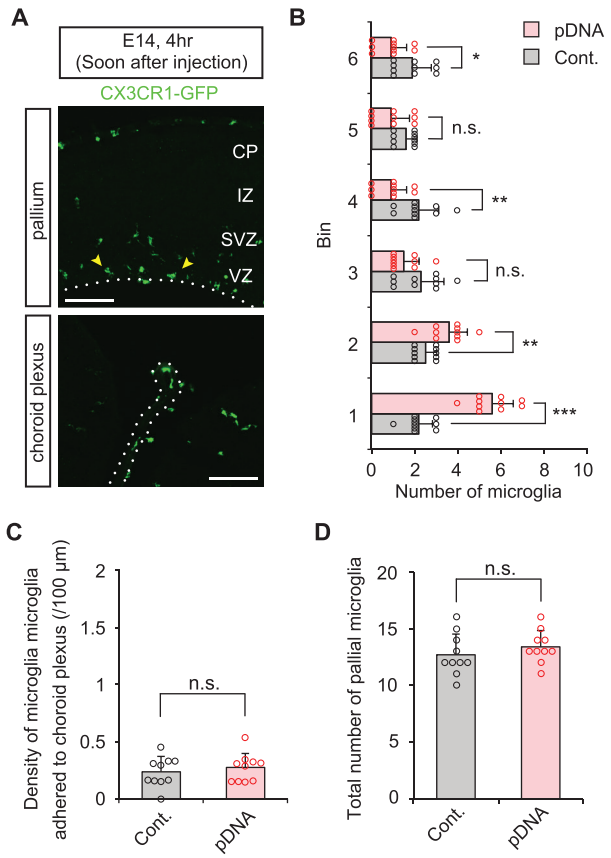

eNeuro Accepted Manuscript

Figure 5

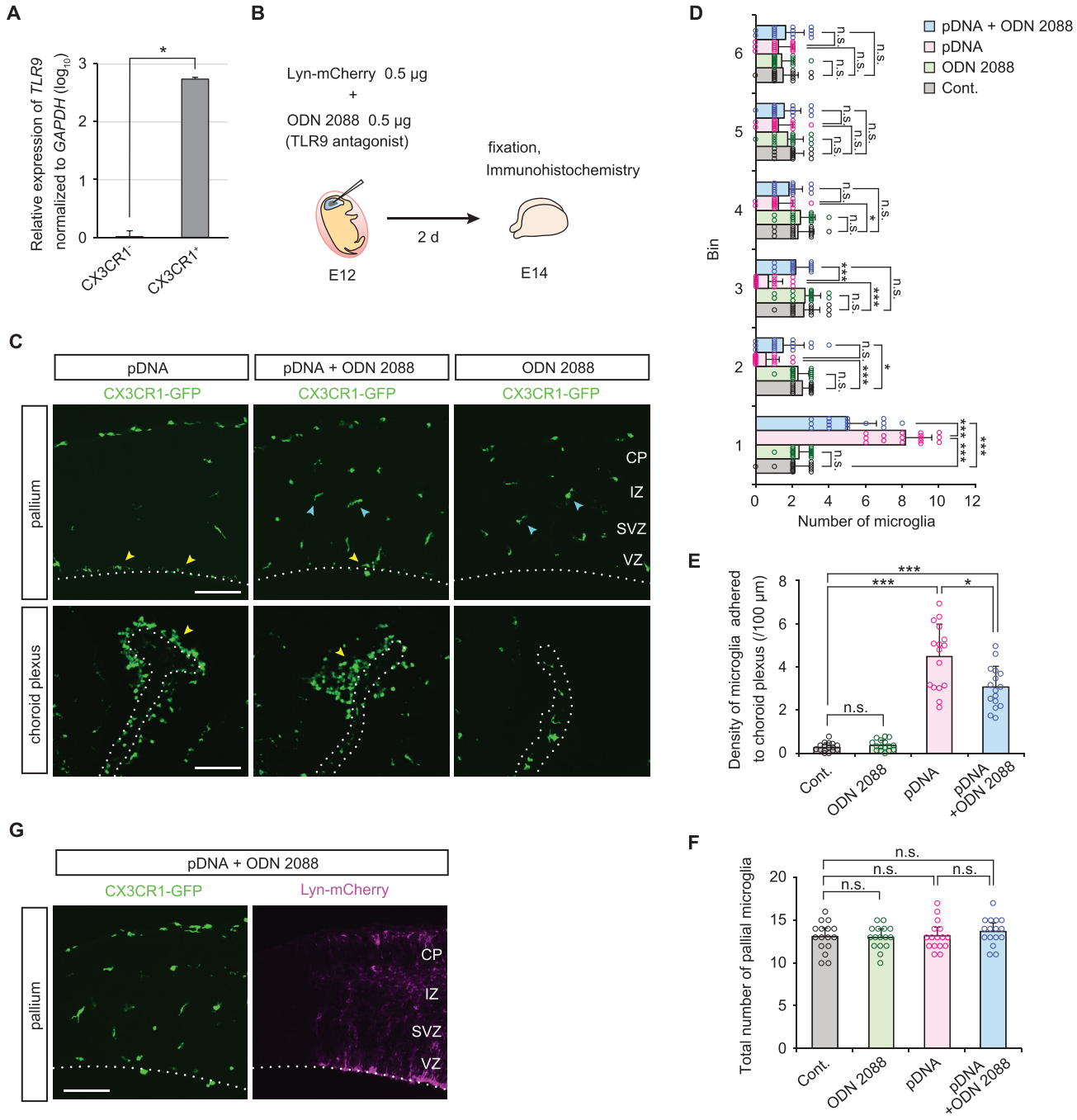

eNeuro Accepted Manuscript

Figure 6

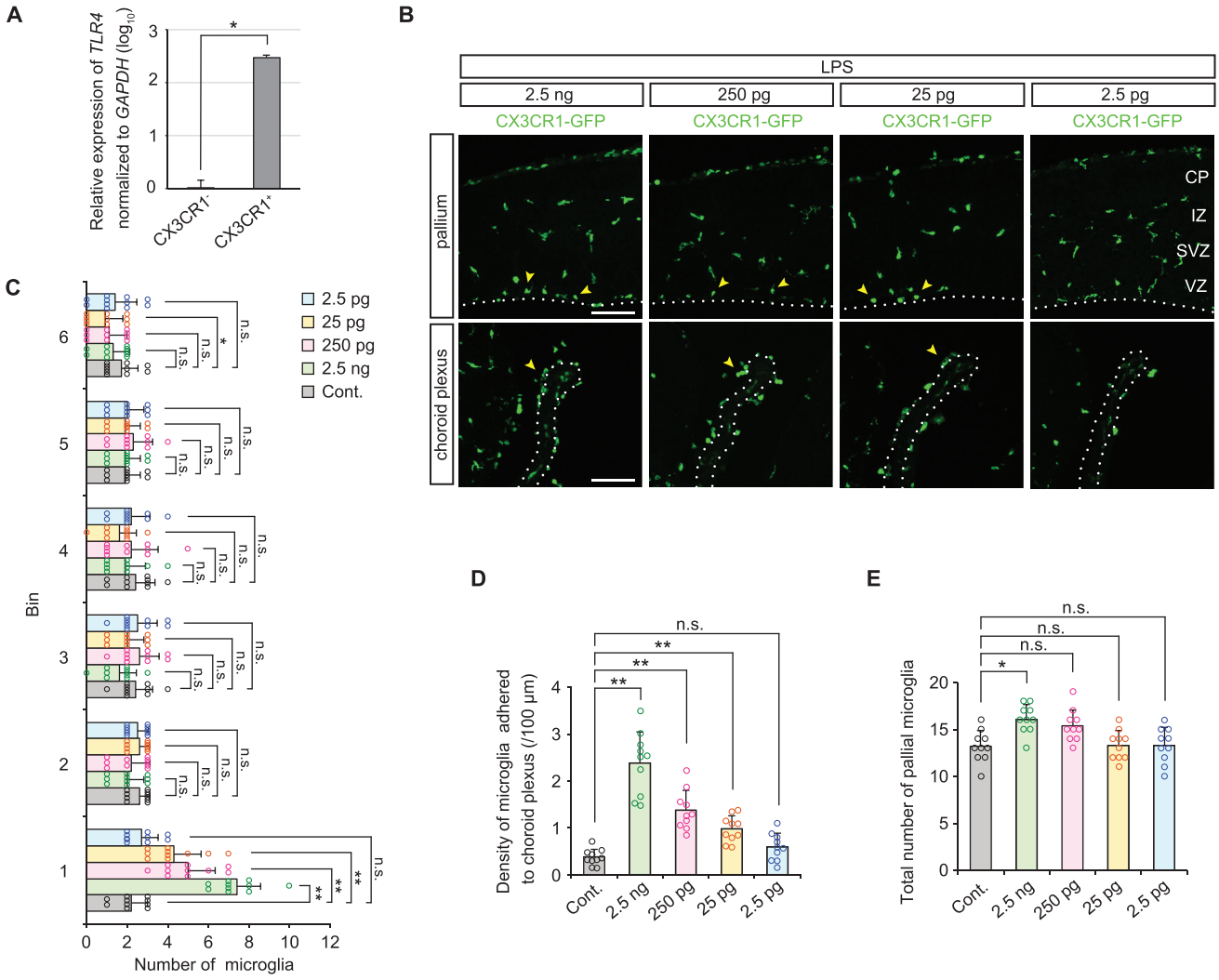

eNeuro Accepted Manuscript

Figure 7

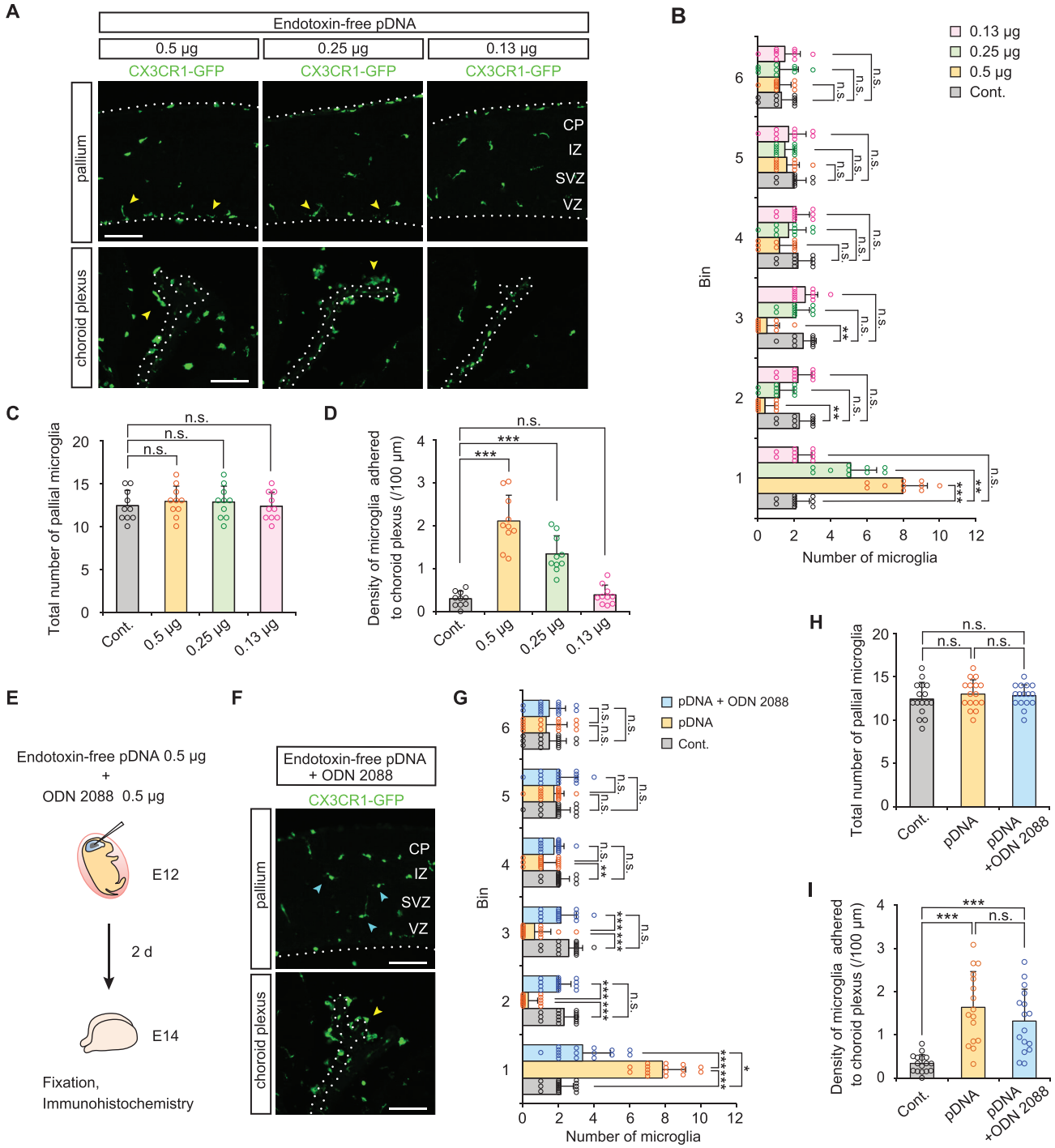

eNeuro Accepted Manuscript

Figure 8